nature electronics

SUPPLEMENTARY INFORMATION

https://doi.org/10.1038/s41928-020-0380-5

In the format provided by the authors and unedited.

An optically driven digital metasurface for programming electromagnetic functions

Xin Ge Zhang[1], Wei Xiang Jiang[1]✉, Hao Lin Jiang[1], Qiang Wang[1], Han Wei Tian[1], Lin Bai[1], Zhang Jie Luo[1], Shang Sun[2], Yu Luo[3], Cheng-Wei Qiu[2]✉ and Tie Jun Cui[1]✉

[1]State Key Laboratory of Millimeter Waves, School of Information Science and Engineering, Southeast University, Nanjing, China. [2]Department of Electrical and Computer Engineering, National University of Singapore, Singapore, Singapore. [3]School of Electrical and Electronic Engineering, Nanyang Technological University, Singapore, Singapore. ✉e-mail: wxjiang81@seu.edu.cn; chengwei.qiu@nus.edu.sg; tjcui@seu.edu.cn

Supplementary Figures

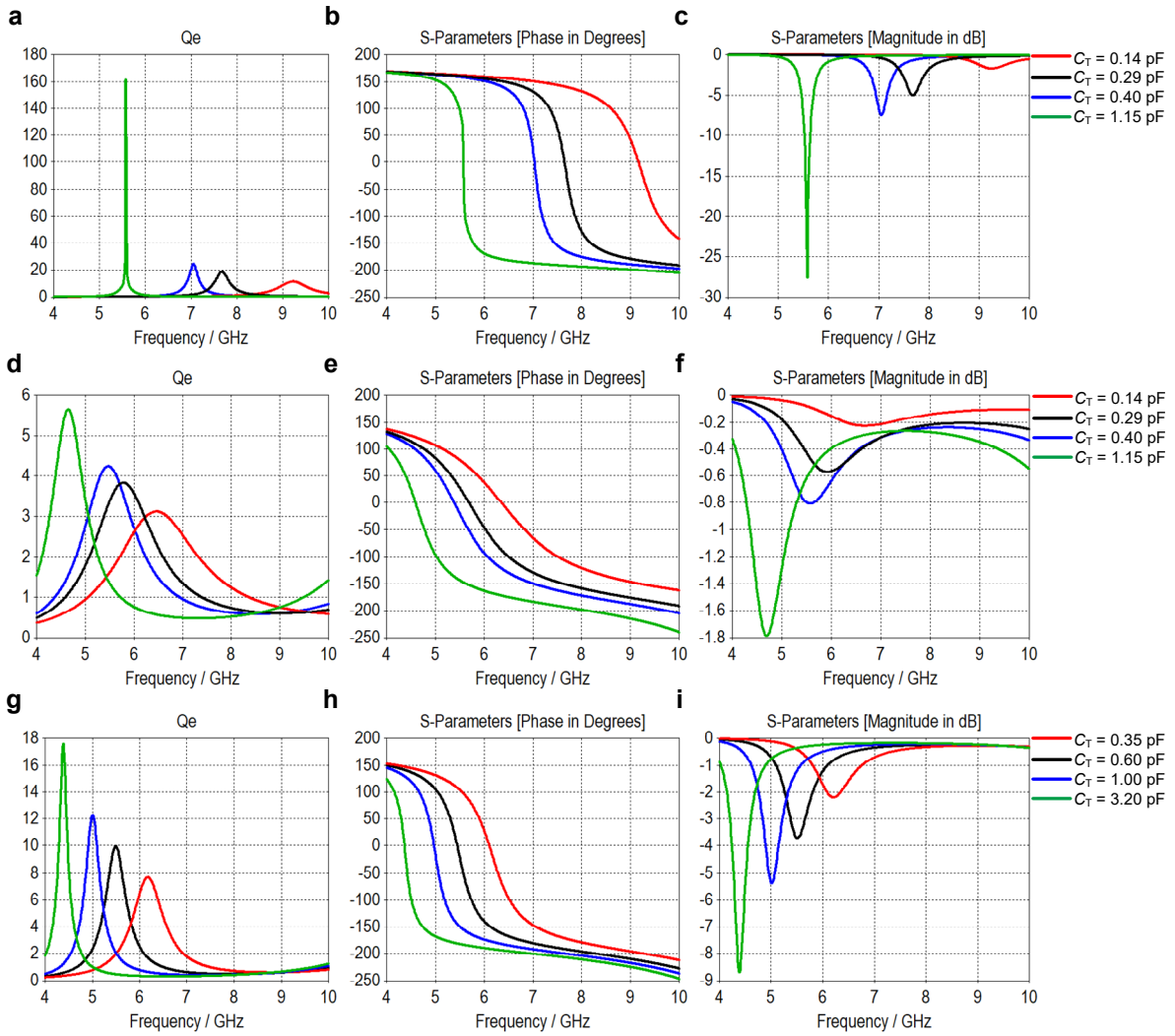

Supplementary Figure 1. Simulated Q factors, reflection phases and reflection amplitudes of the designed ME with different configurations. a-c, Q factors, reflection phases and reflection amplitudes of ME with h = 1.0 mm for different capacitances. **d-f**, Q factors, reflection phases and reflection amplitudes of ME with h = 3.0 mm for different capacitances. **g-i**, Q factors, reflection phases and reflection amplitudes of ME loaded with "Skyworks SMV2020-079LF" varactor of R_S = 2.5 Ω, L_S = 0.7 nH, and a variable capacitance C_T. Here, the four capacitance values are 3.20, 1.00, 0.60, and 0.35 pF.

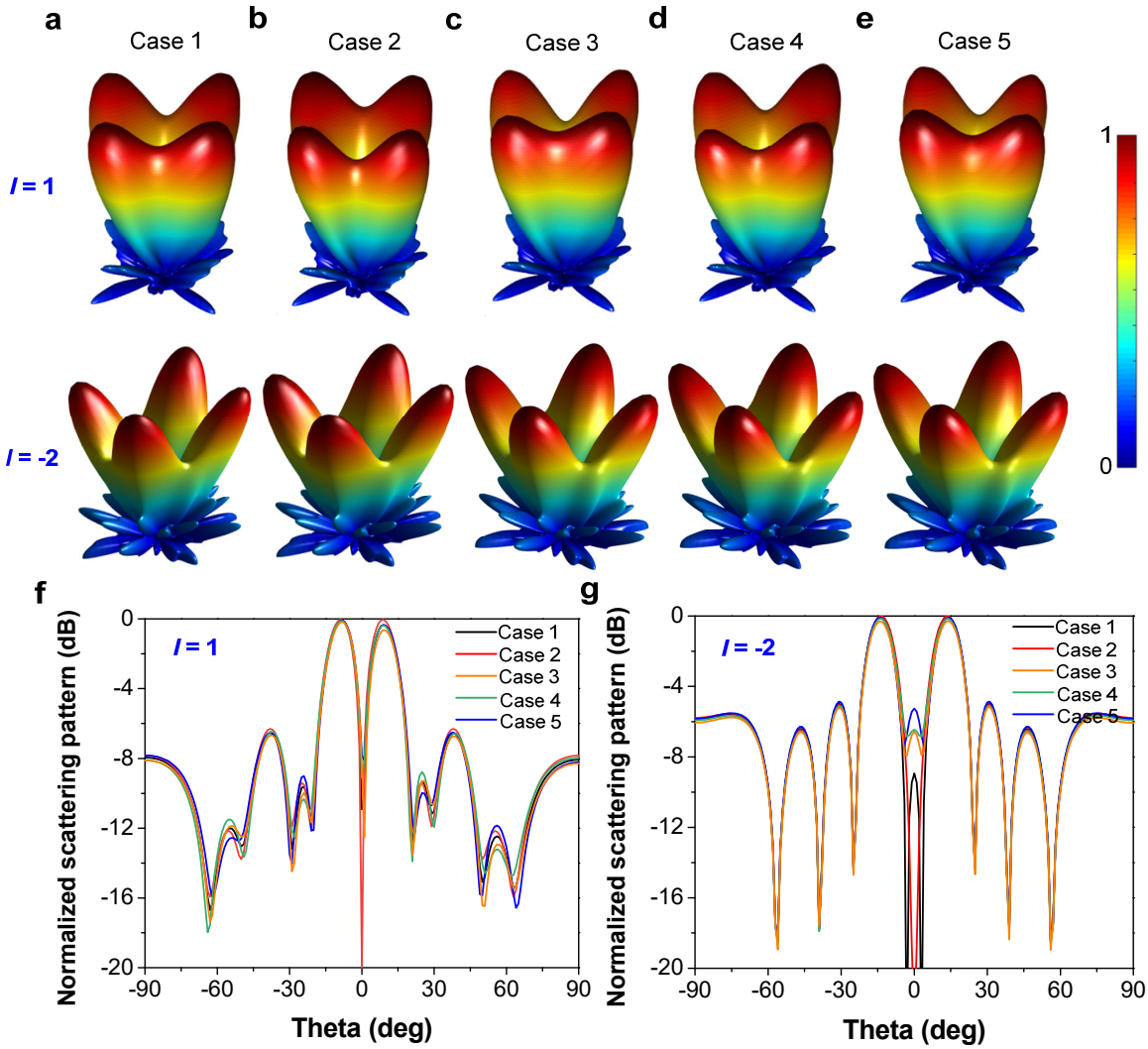

Supplementary Figure 2. Simulated vortex beams of l = 1 and -2 modes at 6.5 GHz under five different cases. a-e, 3D vortex beams of l = 1 and -2 modes under Cases 1, 2, 3, 4, and 5, respectively. **f**,**g**, 2D vortex beams of l = 1 and -2 modes under the five cases, respectively, in which Case 1 is a real case corresponding to the CST simulation; Case 2 is an ideal case with the uniform amplitude distribution; in Case 3, the amplitude differences of the four MEs are larger; Cases 4 and 5 are the cases with two types of introduced phase perturbations.

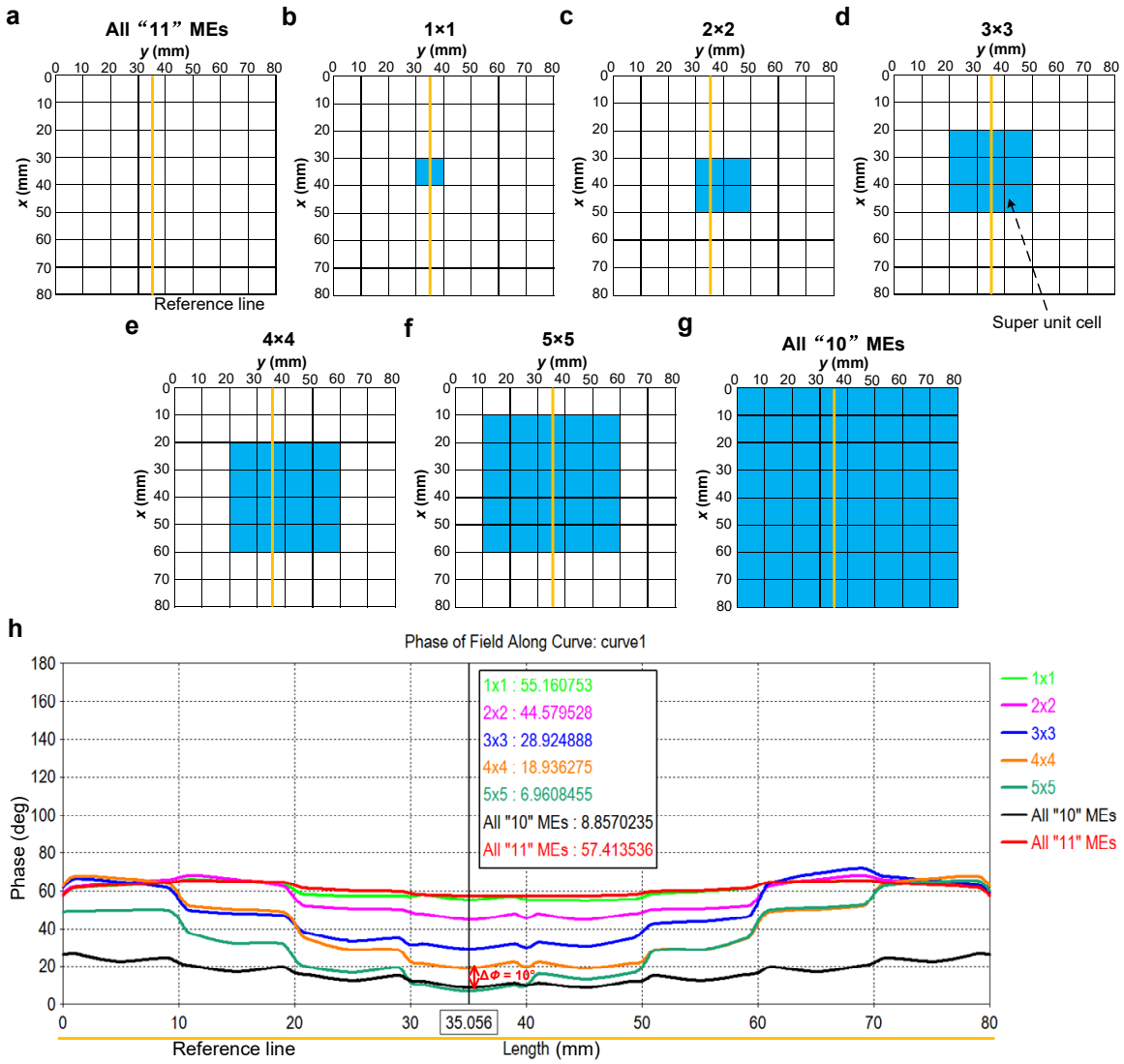

Supplementary Figure 3. Schematics of seven metasurfaces with different configurations and the simulated phases of electric fields at 6.5 GHz on the reference line. a,**g**, Two uniform metasurfaces containing 8×8 “11” and 8×8 “10” digital MEs, respectively. **b**-**f**, Five metasurfaces, in which the super unit cells contain 1×1, 2×2, 3×3, 4×4, and 5×5 “10” MEs, respectively. **h**, Simulated phases of electric fields at 6.5 GHz on the reference line for these seven metasurfaces.

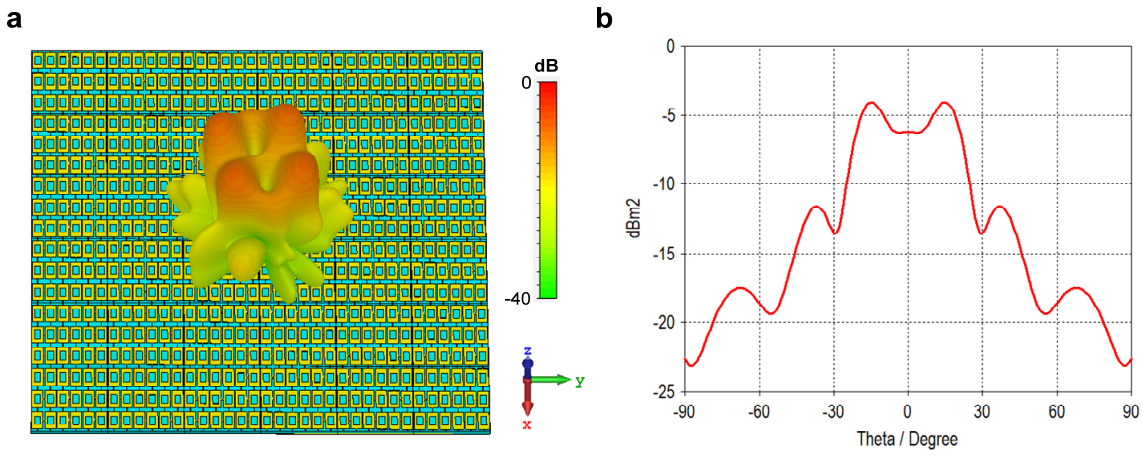

Supplementary Figure 4. Simulated vortex beam with *l* = -2 mode of the metasurface consisting of 6×6 super unit cells, each of which contains 3×3 designed MEs. a, 3D vortex beam of the metasurface at 6.5 GHz. **b**, 2D vortex beam of the metasurface at 6.5 GHz.

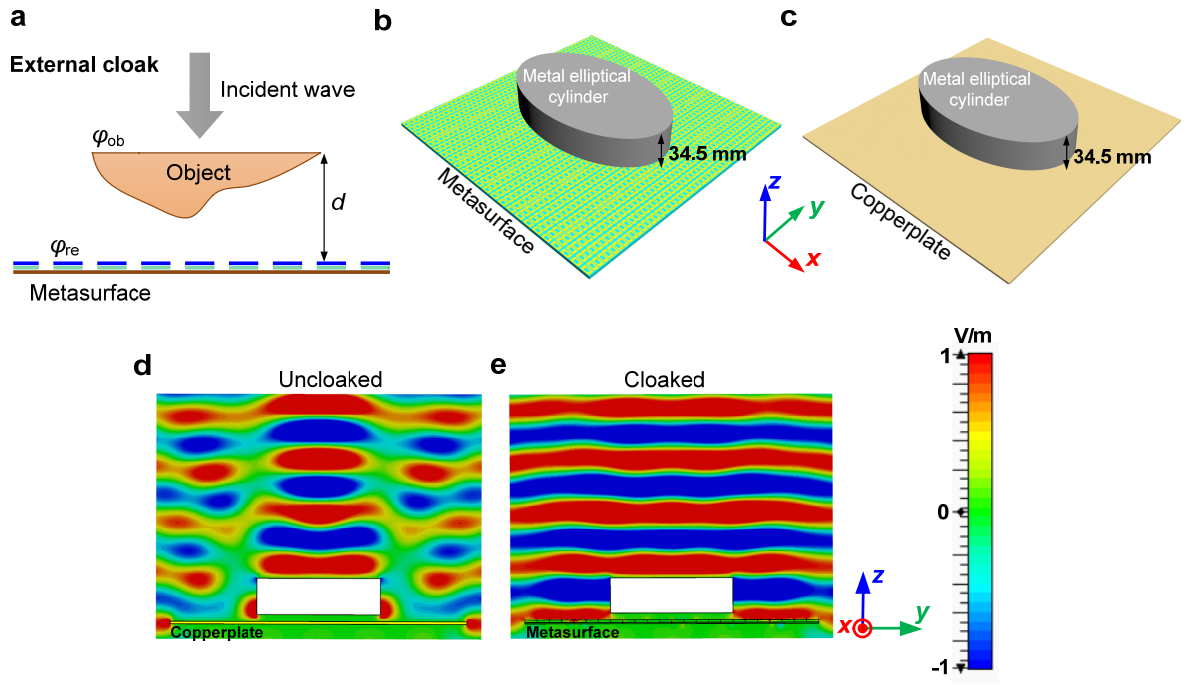

Supplementary Figure 5. Schematic diagram of the proposed metasurface external cloak and simulated cloaking performance at 7.0 GHz. a, Schematic diagram of the metasurface external cloak. **b**, A demonstration example of cloaking a metallic elliptical cylinder on top of the reflective metasurface. **c**, As a comparison, the same elliptical cylinder is located on top of a copperplate. **d**,**e**, Simulated electric field intensity distributions of E_y component on the *y*-*z* plane at 7.0 GHz for Uncloaked-case and Cloaked-case, respectively. It is obvious that the wavefront of scattering waves is restored perfectly for the Cloaked-case.

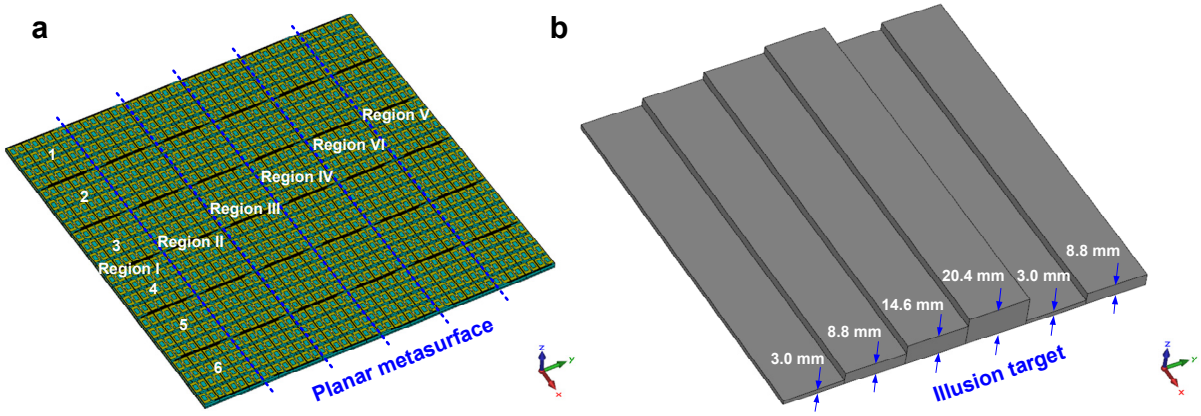

Supplementary Figure 6. Microwave illusion. **a**, Planar metasurface used to realize microwave illusion, which can be divided into six regions along the *y* direction, and each region contains six subarrays along the *x* direction. **b**, Corresponding illusion target. The height of first step of the target ladder is set as 3.0 mm, and hence the heights of other steps of the target ladder is calculated as 8.8, 14.6, 20.4, 3.0, and 8.8 mm, respectively.

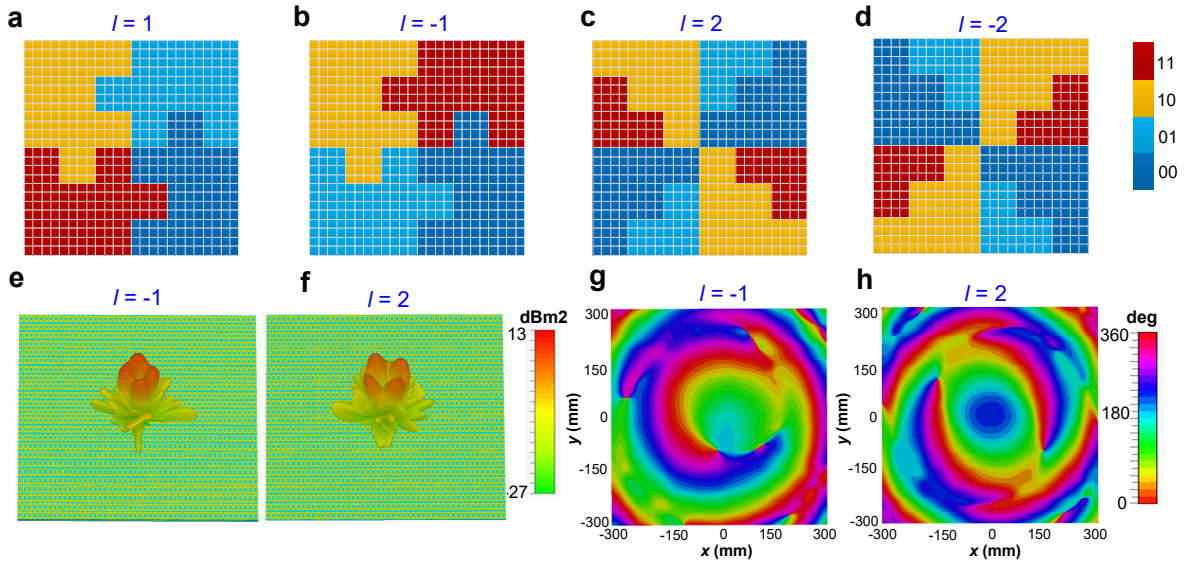

Supplementary Figure 7. Metasurface-based dynamic vortex beam generator. a-d, Four coding patterns on the metasurface for generating vortex beams carrying OAM with modes of l = 1, -1, 2, and -2, respectively. **e**,**f**, Simulated 3D vortex beams of l = -1 and 2 modes at 6.5 GHz, respectively. It is obvious that each beam has a hollow occurring in its center. **g**,**h**, Simulated phase distributions of electric field E_y component on the x-y plane of vortex beams with l = -1 and 2 modes, respectively. We see clearly that there are two spiral-like phase distributions with reverse rotations on the monitoring plane.

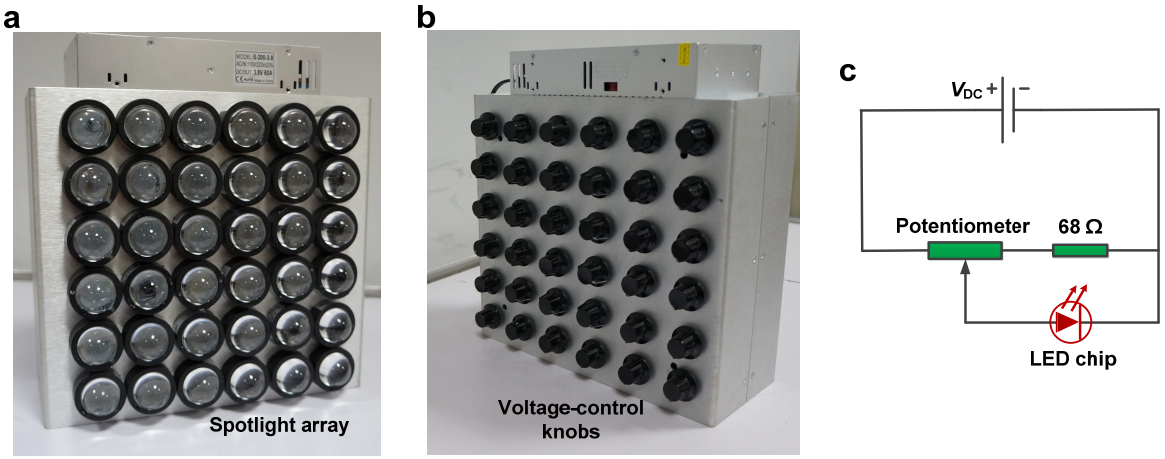

Supplementary Figure 8. Fabricated light source. a,**b**, Front and back views of the fabricated light source array, respectively. **c**, Principle diagram of the designed light-intensity control circuit.

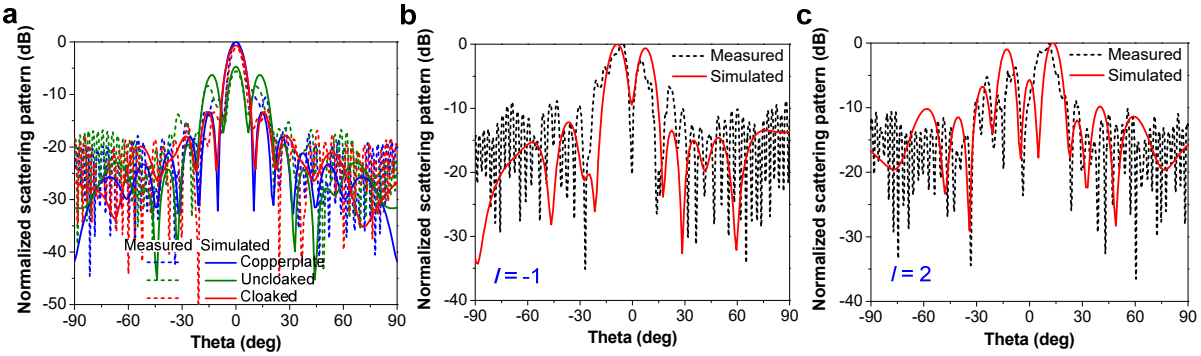

Supplementary Figure 9. Measured results of OIDP. a, Measured and simulated 2D scattering patterns for the Uncloaked-case, Cloaked-case and copperplate at 7.0 GHz. **b**,**c**, Measured and simulated 2D scattering patterns of the vortex beams with l = -1 and 2 modes at 6.5 GHz, respectively.

Supplementary Table

Supplementary Table 1. Values of the reflection amplitudes and reflection phases of four digital MEs in the five different cases. Above and below of the slash indicate the reflection amplitude and reflection phase, respectively.

	Case 1	Case 2	Case 3	Case 4	Case 5
00	0.96 / -172	0.96 / -172	0.93 / -172	0.96 / -172	0.96 / -172
01	0.85 / -82	0.96 / -82	0.75 / -82	0.85 / -92	0.85 / -70
10	0.89 / 8	0.96 / 8	0.84 / 8	0.89 / 0	0.89 / 18
11	0.98 / 98	0.96 / 98	1.00 / 98	0.98 / 98	0.98 / 95

Supplementary Note

Supplementary Note 1. Details on optimization process of the Q factor of ME

As analyzed in the Methods, Q factor determines the rate of phase change and reflectivity of ME. Thus, we need to optimize the Q factor of ME to achieve the required phase tuning and reflectivity in the designed frequency range. Because the magnetic coupling between the top metallic layer and ground is related to the height of ME, we can achieve different Q factors through changing the ME height[1]. We perform a great deal of simulations to investigate the Q factors of ME with different heights. From Supplementary Fig. 1a, it is obvious that the Q factors of ME with different capacitances are all high at resonant frequencies when the height h is set as 1.0 mm. In particular, the Q factor of ME in resonance is larger than 160 when the capacitance C_T = 1.15 pF. Thus, the maximum phase shift range can over 330°, as seen in Supplementary Fig. 1b. However, the reflection phase changes very fast near the resonant frequency. In addition, the reflection amplitudes of ME are very low at resonant frequencies, as depicted in Supplementary Fig. 1c. When h is tuned to 3.0 mm, the Q factors of ME with different capacitances are all below 4.3 in the frequency range of 5-8 GHz, as shown in Supplementary Fig. 1d. With very low Q factor, ME can achieve high reflectivity and flat phase change curve, but the maximum phase difference is just 220°, as illustrated in Supplementary Fig. 1e,f. In these two cases, the other structure parameters of ME in Fig. 2b remain unchanged. Hence, we can conclude that if we want to achieve a large phase tuning range, the Q factor of ME should be high in the designed frequency range; if we require a high reflectivity and a linearly phase shift, the low Q factor is preferred.

On the hand, according to equation (4) in the Methods, we know that the reflection coefficient S_{11} of ME is determined by R_{eff}, L_{eff} and C_{eff}. Thus, the varactor with different capacitances, parasitic inductances and resistances will affect S_{11} of ME. Because S_{11} is related to the Q factor, the used varactor with different parameters can change the Q factor of ME. As an example, we present the simulated Q factors of ME with the loaded varactor ("Skyworks SMV2020-079LF" varactor) of R_S = 2.5 Ω, L_S = 0.7 nH and the variable capacitance C_T (tuning from 3.2 to 0.35 pF), as shown in Supplementary Fig. 1g. Comparing with the Q factors in Fig. 2f, it is obvious that the Q factors of ME with the "Skyworks

SMV2020-079LF" varactor is larger. Thus, ME has a large phase tuning range and a low reflectivity, as seen in Supplementary Fig. 1h,i. Overall, we are able to obtain an optimized Q factor for required phase tuning in the designed frequency range through optimizing the height of ME and adopting the appropriate varactor.

In our design, we aim to construct a ME working within 5-8 GHz with its reflection amplitude over -3 dB in the operating band. Moreover, we require that the realized ME can achieve more than 270° phase shift and the relative bandwidth of 180° phase change exceeds 35%. To balance the phase tuning and reflectivity, we finally set the height of ME as 2.0 mm and adopt the "MA46H120" varactor. In such a case, the Q factors of ME with different capacitances change between 4.5 and 10 in the frequency range of 5-8 GHz, as shown in Fig. 2f. With these optimized Q factors, the requirement of large phase shift, wideband tuning and high reflectivity can be realized in the designed frequency band, as discussed in the main text.

Supplementary Note 2. Influence of amplitude change on the metasurface performance

For the designed optically interrogated metasurface, the reflection amplitude of ME is changed slightly during the phase tuning, as shown in Fig. 2e of the main text. In general, for phase-type dynamic metasurfaces, we hope that the amplitude of ME remains unchanged during the phase tuning. To evaluate the effect of amplitude change on our metasurface performance, we perform some numerical simulations and analyses. Because the required phase distribution of the vortex-beam generation is more complicated than those of external cloaking and illusion, the vortex phenomenon is more sensitive to the amplitude change than the other two functionalities. Hence, we take the vortex-beam generation as an example to further investigate the effect of amplitude inhomogeneity on the metasurface performance.

We consider three cases of different amplitude distributions. Case 1 is the real case, in which the reflection amplitudes and reflection phases of “00”, “01”, “10” and “11” digital MEs are set as actual values obtained from the CST simulation. Case 2 is an ideal case that has the uniform amplitude distribution. As a further comparison, in Case 3, the amplitude differences of the four MEs are larger. The reflection phases of the four MEs in Cases 2 and 3 are identical to those in Case 1. The values of the reflection amplitudes and reflection phases of “00”, “01”, “10” and “11” digital MEs in the three cases are listed in Supplementary Table 1. According to the rotated phase distributions shown in Supplementary Fig. 7a,d, we give the simulated 3D vortex beams of l = 1 and -2 modes at 6.5 GHz under the three different cases, as shown in Supplementary Fig. 2a-c, respectively. It is obvious that the vortex beams of the real case are very similar to those of the ideal case. Moreover, the beams maintain the well vortex characteristics in Case 3. To display the differences of the vortex beams more intuitively, we present the 2D vortex beams of l = 1 and -2 modes under the three different cases, as plotted in Supplementary Fig. 2f,g, respectively. We observe that nonuniform amplitude distributions in Cases 2 and 3 cause slight distortions of the vortex beams, but each beam still has a hollow occurring in its center, which is consistent well with the feature of the vortex beam. All numerical results indicate that the amplitude change has little influence on the vortex-beam generation. Because the external cloaking and illusion have simpler phase distributions, the influence will be smaller. Thus, the effect of amplitude change of the designed ME on the metasurface performance is small and can be acceptable.

Supplementary Note 3. Effect of imperfect phase distribution on the metasurface performance

In experiments, ambient light as well as the stability and homogeneity of light source may affect the phase response of MEs, thus interfering the phase distribution of metasurface. To minimize the interference from these unfavorable factors, our experiments are carried out in a microwave chamber with weak ambient light and the used light source has high stability and homogeneity. Therefore, the interference of these factors on the metasurface is small, but it still exists. We also take the vortex-beam generation as example to study the performance of the designed metasurface when unfavorable factors slightly interfere with its ideal phase distribution. For comparisons with Case 1, we take two other cases (Case 4 and Case 5, see Supplementary Table 1), in which the reflection amplitudes of four MEs are the same as those in Case 1, but the phase difference between two adjacent digital MEs is not 90°. Thus, in Cases 4 and 5 the phase distributions for generating the vortex beams are imperfect. The simulated 3D vortex beams of l = 1 and -2 modes at 6.5 GHz under Case 4 and Case 5 are illustrated in Supplementary Fig. 2d,e, respectively. It is clear that the shapes of vortex beams in these two cases are nearly identical to those in Case 1. From Supplementary Fig. 2f,g, we observe that the curves of 2D vortex beams of the three cases match well. Hence, the imperfect phase distribution has little effect on the vortex-beam generation, and the effect will be less for the external cloaking and illusion due to their simpler phase distributions. We can conclude that when the pre-designed phase distribution on the metasurface is suffered to a minor interference, the metasurface can still maintain good performance.

Supplementary Note 4. Effect of ME numbers in one super unit cell on the metasurface performance

In digital coding metasurfaces, the super unit cell consisting of $N\times N$ identical digital MEs is constructed to mimic the infinitely large periodic boundary condition that are adopted in the simulation of a single ME, thus helping coding metasurfaces produce the accurate phase response[2]. Here, we analyze the effect of the number of the designed MEs in a super unit cell on the metasurface performance. Because the phase distribution on metasurface determines its function, the accuracy of reflection phase of ME is very important to ensure the metasurface performance. Hence, we first investigate quantitatively the influence of the number of MEs in one super unit cell on generating accurate phase response.

We first consider two uniform metasurfaces that contain 8×8 "11" and 8×8 "10" digital MEs, as schematically shown in Supplementary Fig. 3a,g, respectively. To observe the phase of electric field on MEs, at y = 35 mm, we set a reference line (orange line) on the top surface of the metasurface. Under y-polarized incidence, the simulated phase of electric field (Ey component) at 6.5 GHz on the reference line for the two metasurfaces are recorded, as shown in red line and black line, respectively, in Supplementary Fig. 3h. It is clear that the phase distribution on each digital ME of each metasurface is nearly the same, because all the digital MEs in each metasurface are identical. But the phases of electric field on the reference line of these two metasurfaces are different from each other due to the different digital states. Now, we consider other cases with inhomogeneous metasurfaces. In Supplementary Fig. 3b, a "10" ME is used to replace one original "11" ME, to mimic the case that the super unit cell just contains one ME. In such a case, the simulated phase of electric field on the reference line is given in Supplementary Fig. 3h (green line). Comparing the green curve with black curve in the region of 30-40 mm, we observe that the phase on the reference line of the "10" ME is obviously different from that of "10" ME in Supplementary Fig. 3g, and the phase deviation $\Delta\Phi$ achieves 47° at the center of "10" ME. The reason is that, in this case, the "10" ME is completely surrounded by the "11" MEs, breaking its original periodic boundary condition, and thus the uncertain EM coupling occurs, which will affect the resonant state of the"10" ME. To reduce this undesirable EM coupling, we should increase the number of MEs in one super unit cell. The other four metasurfaces whose the super unit cells contain 2×2, 3×3, 4×4,

and 5×5 “10” MEs are shown in Supplementary Fig. 3c-f, respectively, and their corresponding phase curves are also plotted in Supplementary Fig. 3h. It is obvious that the phase deviation $\Delta\Phi$ decreases as the number of “10” MEs increases.

As a demonstrated example, we construct a metasurface that has 6×6 super unit cells, each of which contains 3×3 designed MEs. The simulated 3D vortex beam with l = -2 mode of the metasurface at 6.5 GHz is shown in Supplementary Fig. 4a. In this case, the metasurface can also generate a vortex beam, but the vortex beam has a poor vortex feature comparing with the vortex beam in Fig. 3f. There is still considerable energy in the center of the vortex beam, as seen in Supplementary Fig. 4b. Hence, arranging more MEs in one super unit cell can improve the accuracy of reflection phase of MEs, thus boosting the metasurface performance. However, the processing cost of the large-scale dynamic metasurface is very high because it has many semiconductor chips. Additionally, a large number of MEs will also increase the difficulty of external controls. From Supplementary Fig. 3h, we see that when the super unit cell has 4×4 MEs, the $\Delta\Phi$ is 10°. In Supplementary Note 3, we have demonstrated that the small phase difference around 10° has little effect on the metasurface performance. Hence, in our design, considering both cost and metasurface performance, and also for providing enough space to integrate photodiodes array, we finally adopt 4×4 MEs to form a super unit cell.

Supplementary Note 5. Generation of vortex beams

The vortex beam has a corkscrew-shaped equal-phase wavefront with an azimuthal-phase dependence exp($il\phi$), which can be generated by introducing a spiral-like phase shift. ϕ is the azimuthal angle and l is the OAM topological charge. Because our metasurface can realize various rotated phase distributions on its aperture by controlling the capacitance values of the loaded varactors in each subarray independently, the metasurface can generate multiple vortex beams of different orders.

Supplementary References

1. Pu, M. et al. Broadband anomalous reflection based on gradient low-Q meta-surface, *AIP Adv.* **3**, 052136 (2013).
2. Liu, S. et al. Frequency-dependent dual-functional coding metasurfaces at terahertz frequencies. *Adv. Opt. Mater.* **4**, 1965-1973 (2016).